PHYSICAL REVIEW B **78**, 214303 (2008)

First-principles approach to chemical diffusion of lithium atoms in a graphite intercalation compound

Kazuaki Toyoura,[1,*] Yukinori Koyama,[2] Akihide Kuwabara,[1] Fumiyasu Oba,[1] and Isao Tanaka[1,3,†]
[1]*Department of Materials Science and Engineering, Kyoto University, Yoshida, Sakyo, Kyoto 606-8501, Japan*
[2]*Innovative Collaboration Center, Kyoto University, Yoshida, Sakyo, Kyoto 606-8501, Japan*
[3]*Nanostructure Research Laboratory, Japan Fine Ceramics Center, Atsuta, Nagoya 456-8587, Japan*
(Received 20 February 2008; revised manuscript received 12 November 2008; published 19 December 2008)

We evaluate mean frequencies for atomic jumps in a crystal from first principles based on transition state theory, taking lithium diffusion by the interstitial and vacancy mechanisms in LiC_6 as a model case. The mean jump frequencies are quantitatively evaluated from the potential barriers and the phonon frequencies for both initial and saddle-point states of the jumps under the harmonic approximation. The lattice vibrations are treated within quantum statistics, not using the conventional treatment by Vineyard corresponding to the classical limit, and the discrepancy between the two treatments is quantitatively discussed. The apparent activation energies and the vibrational prefactors of the mean jump frequencies essentially depend on temperature, unlike in the case of the classical approximation. The discrepancies of the activation energies correspond to the changes in zero-point vibrational energy at 0 K, and there remains the effect even at 1000 K. With regard to the vibrational prefactors, the classical approximation extremely overestimates the prefactors at low temperatures while the discrepancies rapidly decrease with increasing temperature, e.g., by 30% at room temperature and by 5% at 1000 K. The calculated chemical diffusion coefficients of lithium atoms by the interstitial and vacancy mechanisms are 1×10^{-11} and 1×10^{-10} $\mathrm{cm^2/s}$, respectively.

DOI: 10.1103/PhysRevB.78.214303 PACS number(s): 66.30.Ny, 66.30.Dn

I. INTRODUCTION

The diffusion of atoms, molecules, and ions plays a key role in many physical and chemical processes, for instance, crystal and film growth, phase transitions, and ionic conduction. It is well known that diffusion fluxes follow Fick's first law.[1] The major issue in research on diffusion is the evaluation of diffusion coefficients under conditions of interest. Molecular-dynamics (MD) simulations are often used to theoretically evaluate the diffusion coefficients.[2,3] In MD simulations, the diffusion coefficients are evaluated from the migration distance of the species in a certain time. In spite of the successes of MD simulations for modeling fast diffusion, the technique is not effective for slow diffusion in crystals. Diffusion in crystals consists of a series of elementary jumps. The mean frequency of the jumps is empirically expressed as

$$\omega = \nu^* \exp\left(-\frac{q}{kT}\right), \tag{1}$$

where k is the Boltzmann constant, T is the temperature, and q is the apparent activation energy. The pre-exponential factor of ν^* and the exponential term are often considered as the jump attempt frequency and the success probability of the jump, respectively. The success probability is very small under the low-temperature condition of $T \ll q/k$. For example, it is less than 10^{-8} for the activation energy of $q=0.5$ eV at room temperature. This means that on average 10^8 trials are necessary for every jump in MD simulations, and the calculation costs are infeasibly expensive.

A statistical-mechanical approach based on transition state theory (TST) (Refs. 4 and 5) is an effective method of evaluating the mean jump frequency in crystals. In this approach, the questions are: what types of jumps happen and how often do they occur? The nudged elastic band (NEB) method[6] is a useful technique for finding migration paths and evaluating potential barriers on the paths. It, however, gives no information on the vibrational prefactor ν^* in Eq. (1). Therefore, the factor ν^* has been often approximated by the Debye frequencies or constant values of 10^{12}–10^{13} $\mathrm{s^{-1}}$ to obtain the mean jump frequency ω.[7–9] Once all jump frequencies for possible jumps in a crystal are obtained, the diffusion behavior can be readily simulated using the kinetic Monte Carlo (KMC) technique, which has been applied even to the nonstoichiometric and disordered systems.[8]

Based on transition state theory, the vibrational prefactors ν^* can be derived from the lattice vibrations at the initial and saddle-point states for the jumps. The following equation formulated by Vineyard[10] has been conventionally used for evaluating the mean jump frequency:

$$\omega = \frac{\prod_{i=1}^{3N} \nu_i^I}{\prod_{i=1}^{3N-1} \nu_i^S} \exp\left(-\frac{\Delta E^{\mathrm{mig}}}{kT}\right), \tag{2}$$

where ΔE^{mig} is the potential barrier, and ν_i^I and ν_i^S are the frequencies of the normal vibrational modes at the initial and saddle points, respectively. However, Eq. (2) is not rigorous because this expression corresponds to just a classical limit of quantum statistics (described later in detail). In many reports on the prefactor ν^*, the eigenfrequencies estimated within the local vibrations around a migrating atom have been applied to Eq. (2).[11,12] Though some researchers have evaluated the prefactor beyond the above framework,[13,14] there are no reports on the first-principles evaluation of the prefactor ν^* based on quantum statistics using the lattice vibrations over the entire cell.

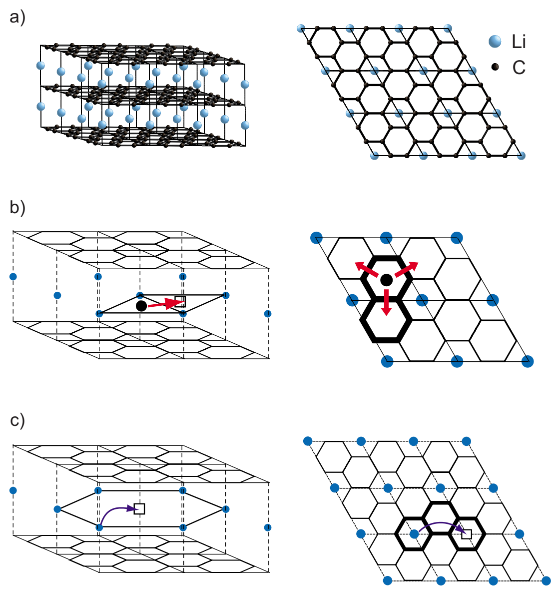

FIG. 1. (Color online) (a) Crystal structure of LiC_6. Schematic drawings of lithium migrations by (b) the interstitial and (c) the vacancy mechanisms.

In the present work, we have focused on the evaluation of mean jump frequencies from first principles in the rigorous manner. The lattice vibrations at the initial and saddle-point states for the jumps are evaluated over the supercell, not confined to the local vibrations near the migrating atom. The lattice vibrations are treated based on quantum statistics, and the validity of the classical approximation [Eq. (2)] is discussed. The chemical diffusion coefficient is finally estimated from the calculated mean jump frequencies. In this paper, a first-stage lithium-graphite intercalation compound (stage-1 Li-GIC) of LiC_6 is taken as a model system, which is widely used for negative electrodes in lithium-ion rechargeable batteries. The diffusion mechanism of lithium atoms in LiC_6 has not been clearly understood in the atomic level, though there are many reports on electrochemical measurements of the lithium diffusion at room temperature.[15]

II. METHODOLOGY

A. Diffusion of Li atoms in LiC_6

The intercalation of lithium atoms into graphite and the structural feature have been well investigated so far.[15–18] Lithium atoms form a superstructure in interlayers of graphite, and the stacking of graphene and lithium layers has periodicity, which is called *staging*. The staging phenomenon is characterized by a periodic sequence of intercalant layers, and the stage number n refers to the number of host layers separating two intercalant layers. In the case of Li-GIC, lithium atoms are inserted into graphite with staging phase transitions repeated, ultimately, to reach the stage-1 LiC_6.

The crystal structure of LiC_6 is shown in Fig. 1(a). Lithium atoms are located in all the interlayers, and form a $(\sqrt{3}\times\sqrt{3})R30°$ superstructure occupying one third of carbon hexagonal sites. According to the literature, the ordering of lithium atoms was reported to be stable up to 715 K,[17] and the deviation of lithium composition from the stoichiometry was less than 1% up to 433 K.[18] In the present study, the diffusion of lithium atoms in LiC_6 is considered to be mediated by the lithium interstitials and vacancies. In this one-component diffusion within a host matrix of graphene sheets, the flux and concentration of lithium atoms are equivalent to those of the defects. The chemical diffusion coefficient of lithium atoms D_{Li} can be, therefore, related to those of the defects D_{defect}. The relation between D_{Li} and D_{defect} is described hereafter.

The chemical diffusion coefficient of lithium atoms D_{Li} is defined by Fick's first law as

$$J_{Li} = -D_{Li}\nabla C_{Li}, \tag{3}$$

where J_{Li} and C_{Li} are the flux and concentration of lithium atoms, respectively. In the lithium excess case, the lithium diffusion is mediated by the lithium interstitials. The interstitial mechanism is examined in this paper. The flux of lithium atoms can be separated into the two contributions, i.e., $J_{Li}=J_{Reg}+J_{Int}$, where J_{Reg} and J_{Int} are the fluxes of lithium atoms at regular and interstitial sites, respectively. The concentration of lithium atoms is also separated into those of lithium atoms at regular and interstitials sites (C_{Reg} and C_{Int}), i.e., $C_{Li}=C_{Reg}+C_{Int}$. Lithium atoms at the regular sites do not migrate in the interstitial mechanism, leading to $J_{Reg}=0$ and $\nabla C_{Reg}=0$. Hence, Eq. (3) can be rewritten as

$$J_{Int} = -D_{Li}\nabla C_{Int}. \tag{4}$$

Equation (4) can be interpreted as the relation between the flux and concentration gradient of interstitials, i.e., Fick's first law of the interstitials. Consequently, D_{Li} by the interstitial mechanism is equal to the chemical diffusion coefficient of the interstitials D_{Int}. In the lithium deficient case, the lithium vacancies mediate the diffusion of lithium atoms. The regular sites are occupied by either lithium atoms or vacancies, $C_{Li}+C_V$=const, where C_V is the concentration of vacancies. Since the concentration of the regular sites is constant, the fluxes of lithium atoms and vacancies follow the relation of $J_{Li}+J_V=0$ (J_V is the flux of vacancies). Therefore, Eq. (3) can be rewritten as

$$J_V = -D_{Li}\nabla C_V. \tag{5}$$

This means that D_{Li} by the vacancy mechanism is equal to that of the vacancies D_V because Eq. (5) can be interpreted as Fick's first law of the vacancies. Consequently, D_{Li} is equal to D_{defect} in both lithium excess and deficient cases.

B. Fluctuation dissipation theorem

The chemical diffusion of the defects can be readily evaluated because of their independent migration, in contrast to the correlative migration of lithium atoms. On the basis of fluctuation dissipation theorem, the chemical diffusion coefficient D in a one-component system within a host matrix is given by a product of the thermodynamic factor Θ and the jump diffusion coefficient, D_J,[8,19]

$$D = \Theta D_J, \tag{6}$$

$$\Theta = \frac{\partial(\mu/kT)}{\partial \ln x}, \tag{7}$$

$$D_J = \lim_{t\to\infty} \frac{1}{2dt} \left\langle \frac{1}{N} \left| \sum_{i=1}^{N} \vec{r}_i(t) \right|^2 \right\rangle, \tag{8}$$

where μ is the chemical potential, x is the ratio of the diffusing atoms to the number of available sites for the atoms in the system, d is the dimension of diffusion field, N is the number of the atoms, and $\vec{r}_i(t)$ is the displacement of the ith atom after time t. D_J is divided into two parts: the diagonal and nondiagonal parts,

$$D_J = \lim_{t\to\infty} \frac{1}{2dt} \left(\frac{1}{N} \sum_{i=1}^{N} \langle |\vec{r}_i(t)|^2 \rangle \right) + \lim_{t\to\infty} \frac{1}{2dt} \left(\frac{1}{N} \sum_{i\neq j} \langle \vec{r}_i(t)\vec{r}_j(t) \rangle \right). \tag{9}$$

D_J consists of the first diagonal part corresponding to the self-diffusion coefficient, D^*, and the second nondiagonal part of the cross-correlation functions between different atoms i and j. Generally, the nondiagonal part is not negligible, including the lithium migration in LiC_6. In contrast, the nondiagonal part is negligible for the migration of the point defects because the small deviation of lithium composition from the stoichiometry leads to the independent migration. According to Henry's law, the thermodynamic factors of the defects, Θ, are unity due to the low concentration, finally leading to $D_{\rm defect} = D^*_{\rm defect}$ ($D^*_{\rm defect}$: self-diffusion coefficient of the defects). $D_{\rm Li}$ is equal to the self-diffusion coefficients of the interstitials and vacancies in the lithium excess and deficient cases, respectively.

C. Transition state theory

The self-diffusion coefficient of independent defects can be evaluated from the jump frequency of the single defect as follows:

$$D^*_{\rm defect} = \frac{1}{2d} \Gamma \alpha^2, \tag{10}$$

where d is the dimension of the diffusion field (=2 for in-plane diffusions), Γ is the total jump frequency of the defect, and α is the jump length. This means that the evaluation of $D_{\rm Li}$ comes down to the estimation of the jump frequencies of the single interstitial and vacancy.

TST has contributed to evaluation of mean frequencies of atomic jumps in solids.[4,19] On the basis of TST, mean frequencies ω of atomic jumps in solids are given by

$$\omega = \frac{kT}{h} \frac{Z_S^{\rm vib}}{Z_I^{\rm vib}} \exp\left(-\frac{\Delta E^{\rm mig}}{kT} \right), \tag{11}$$

where h is Planck's constant, and $Z_I^{\rm vib}$ and $Z_S^{\rm vib}$ are the vibrational partition functions at the initial and saddle-point states, respectively. Note that the vibrational partition function at the initial is evaluated with $3N$ degrees of freedom while that at the saddle point is with $3N-1$ degrees; the migration coordinate is excluded. Using the relation between partition functions and free energies,

$$F^{\rm vib} = -kT \ln Z^{\rm vib}, \tag{12}$$

the mean jump frequency is rewritten by

$$\omega = \frac{kT}{h} \exp\left(-\frac{\Delta E^{\rm mig} + \Delta F^{\rm vib}}{kT} \right), \tag{13}$$

$$\Delta F^{\rm vib} = F_S^{\rm vib} - F_I^{\rm vib}. \tag{14}$$

Consequently, the evaluation of the mean jump frequency comes down to the estimation of the two changes in potential energy and vibrational free energy from the initial to the saddle point for the jump, $\Delta E^{\rm mig}$ and $\Delta F^{\rm vib}$.

In the present study, the lattice vibrations are treated under the harmonic approximation. Based on quantum statistics, vibrational free energies are described as

$$F^{\rm vib} = \sum_i \left\{ \frac{1}{2} h\nu_i + kT \ln\left[1 - \exp\left(-\frac{h\nu_i}{kT} \right) \right] \right\}, \tag{15}$$

where ν_i is the vibrational frequency of the ith normal mode. The classical limit of vibrational free energies is expressed as

$$F^{\rm vib} = kT \sum_i \ln\left(\frac{h\nu_i}{kT} \right). \tag{16}$$

Using the classical vibrational free energy of Eq. (16), the mean jump frequency is approximated as the conventional expression formulated by Vineyard[10] [Eq. (2)]. In this paper, the discrepancy between the quantum and classical treatments is quantitatively evaluated, and the validity of the classical approximation is discussed.

D. Computational conditions

The first-principles calculations were performed using the projector augmented wave (PAW) method as implemented in the VASP code.[20] A $3\times3\times2$ supercell of LiC_6 was used, containing 18 lithium atoms and 108 carbon atoms. A lithium interstitial or vacancy was introduced into the supercell. The local-density approximation (LDA) (Ref. 21) was used for the exchange-correlation term. The plane-wave cutoff energy was 350 eV. $2s$ and $2p$ orbitals were treated as valence states for both lithium and carbon. Integration in the reciprocal space was made using a $3\times3\times6$ k-point mesh in the Brillouin zone by the Monkhorst-Pack scheme.[22] The NEB method was used for finding the migration paths and evaluating the potential barriers on the paths.[6] For the migration-path search, atom positions were fully optimized until the residual forces became less than 0.02 eV/Å. The lattice vibrations were evaluated under the harmonic approximation using the frozen phonon method, as implemented in the "FROPHO" code.[23] Each atom in the supercell was displaced by a small amount (0.01 Å in the present work) in the x, y, or z direction to obtain all the interatomic force constants. Since the vibrational frequencies are sensitive to the residual forces of the structures without the displacement, the structures were precisely optimized with the convergence of 10^{-5} eV/Å of the residual forces.

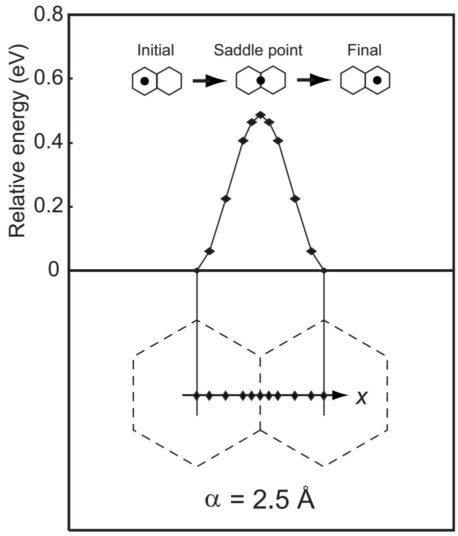

FIG. 2. (Bottom) Migration path and (top) energy profile along the path by the interstitial mechanism. The schematic drawings of the migration path are inserted in the figure. The hexagons denote the hexagonal network of carbon atoms [see also Fig. 1(b)].

III. RESULTS

A. Interstitial mechanism

1. Migration path and potential barrier

Figure 1(b) shows the schematic drawings of lithium migration by the interstitial mechanism. An interstitial is located at an unoccupied site of carbon hexagons, and surrounded by the three lithium atoms at regular sites. It has three neighboring interstitial sites and jumps into one of them. The calculated migration path and energy profile along the path are shown in Fig. 2. The energy profile shows that the interstitial jump goes through a saddle-point state. The saddle point corresponds to just the middle point for the migration when the interstitial is located on the borders of the two carbon hexagons. The mean jump frequency ω_{Int} from the initial interstitial site to the neighboring site (jump Int) is needed to evaluate the diffusion coefficient by this mechanism. The calculated potential barrier ΔE^{mig} is 0.48 eV.

2. Change in vibrational free energy

Figure 3 shows the calculated phonon band structures and vibrational spectra at (a) the initial (equal to the final) and (b) the saddle-point states. The horizontal axes of the band structures stand for the path in the reciprocal space for the supercell (a $3\times3\times2$ cell of primitive LiC_6). Each band structure has 381 modes for the 127 atoms in the supercell. The major difference between the two band structures is whether an imaginary mode appears or not. At the initial state, all the vibrational modes have real frequencies while an imaginary mode appears at the saddle-point state. The imaginary mode corresponds to the picture that the potential energy at the saddle-point state is the local maximum only to the migration coordinate. The flat imaginary band indicates that the mode corresponding to the migration is sufficiently localized in the supercell.

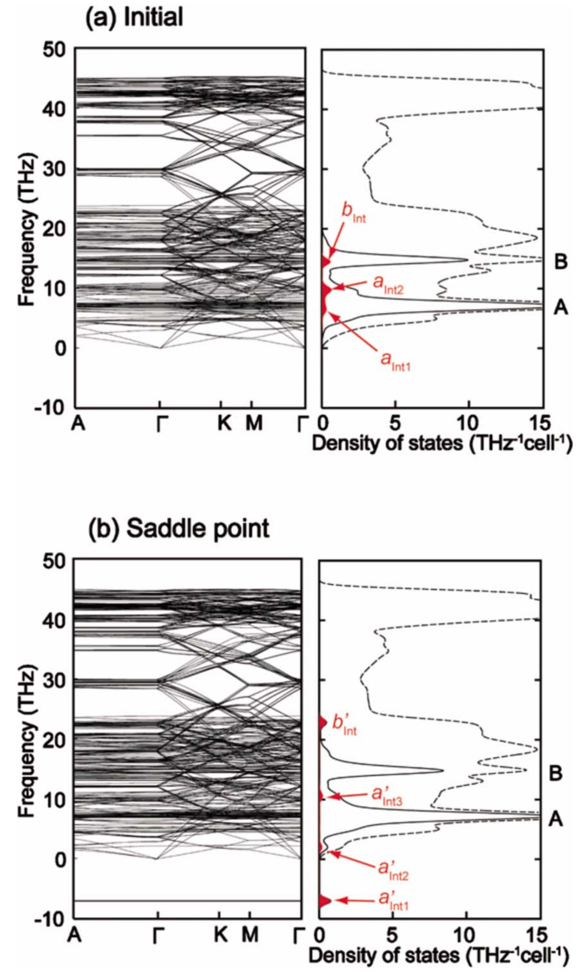

FIG. 3. (Color online) Calculated phonon band structures and vibrational spectra at (a) the initial and (b) the saddle-point states in the interstitial mechanism. The total spectrum, the contribution of all lithium atoms, and that of the migrating lithium atom are expressed by broken line, solid line, and red filled region (indicated by arrows), respectively. Imaginary frequencies are expressed as negative values.

In the vibrational spectra, the total spectrum (broken line) and the contribution of all the lithium atoms (solid line) and the interstitial (filled region) are shown. The contribution of the lithium atoms are focused hereafter. At the initial state, there are two major peaks (A at 7 THz and B at 15 THz). Investigating the corresponding normal-mode coordinates, peaks A and B are attributed to the in-plane and perpendicular vibrations of the lithium atoms, respectively. The contribution of the interstitial at the initial state has three peaks (peaks $a_{\mathrm{Int}\,1}$, $a_{\mathrm{Int}\,2}$, and b_{Int}) at 6.5, 9.7, and 14.5 THz, respectively. Peaks $a_{\mathrm{Int}\,1}$ and $a_{\mathrm{Int}\,2}$ are attributed to the in-plane vibration while peak b_{Int} is due to the perpendicular. At the saddle-point state, drastic changes appear in the interstitial contribution. First of all, one imaginary mode (peak $a'_{\mathrm{Int}\,1}$) appears. This mode exactly corresponds to the in-plane vibration in the direction of the interstitial jump. There are three peaks with real frequency at 2.0, 10.5, and 22.9 THz

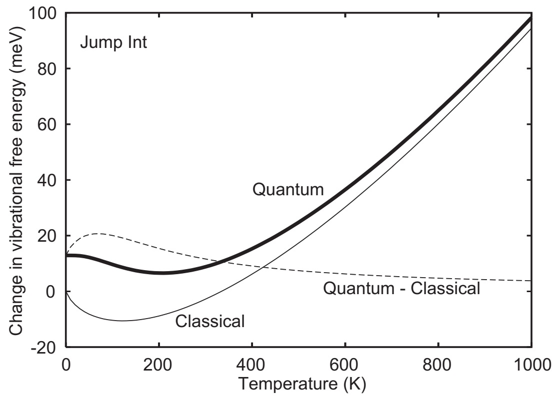

FIG. 4. Changes in vibrational free energy ΔF^{vib} for jump Int as a function of temperature, evaluated in (thick line) quantum and (thin line) classical statistics. The discrepancy is also shown in the figures by broken line.

(peaks $a'_{\mathrm{Int}\,2}$, $a'_{\mathrm{Int}\,3}$, and b'_{Int}). The former two are attributed to the in-plane vibration while the last is to the perpendicular vibration. The details of the vibrational modes will be discussed later.

Figure 4 shows the changes in vibrational free energy ΔF^{vib} based on quantum and classical statistics. The differences between both statistics are also shown in the figure. At 0 K, the quantum ΔF^{vib} has a finite value of the change in zero-point vibrational energy $\Delta E^{\mathrm{vib}}_{\mathrm{zero}}$ while the classical one is exactly zero. The discrepancy between both statistics is 13 meV at 0 K, and it remains 12 meV at room temperature.

3. Mean jump frequency and diffusion coefficient

It is now possible to evaluate the mean jump frequency from the potential barrier, ΔE^{mig}, shown in Fig. 2, and the change in vibrational free energy, ΔF^{vib}, in Fig. 4. Figure 5 shows the calculated mean jump frequency, ω_{Int}, based on quantum statistics. For example, the frequency is $6 \times 10^4\ \mathrm{s}^{-1}$ at room temperature. The total jump frequency of the interstitial mechanism, Γ_{Int}, is $3\omega_{\mathrm{Int}}$ because of three possible migration paths per interstitial. Figure 6 shows the calculated chemical diffusion coefficient of lithium atoms D_{Li} by the interstitial mechanism as a function of (a) temperature and (b) the inverse of temperature. At room temperature, the diffusion coefficient is $1 \times 10^{-11}\ \mathrm{cm}^2/\mathrm{s}$. The apparent activation energy Q (100–1000 K) is 0.51 eV, which is larger than the potential barrier of jump Int ($\Delta E^{\mathrm{mig}} = 0.48$ eV). This results from the major contribution of the change in zero-point vibrational energy $\Delta E^{\mathrm{vib}}_{\mathrm{zero}}$ at low temperatures, which is unique to quantum statistics beyond the concept of classical statistics.

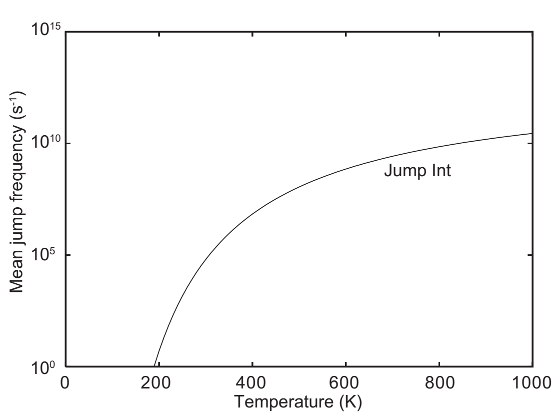

FIG. 5. Calculated mean frequencies of jump Int as a function of temperature using quantum statistics.

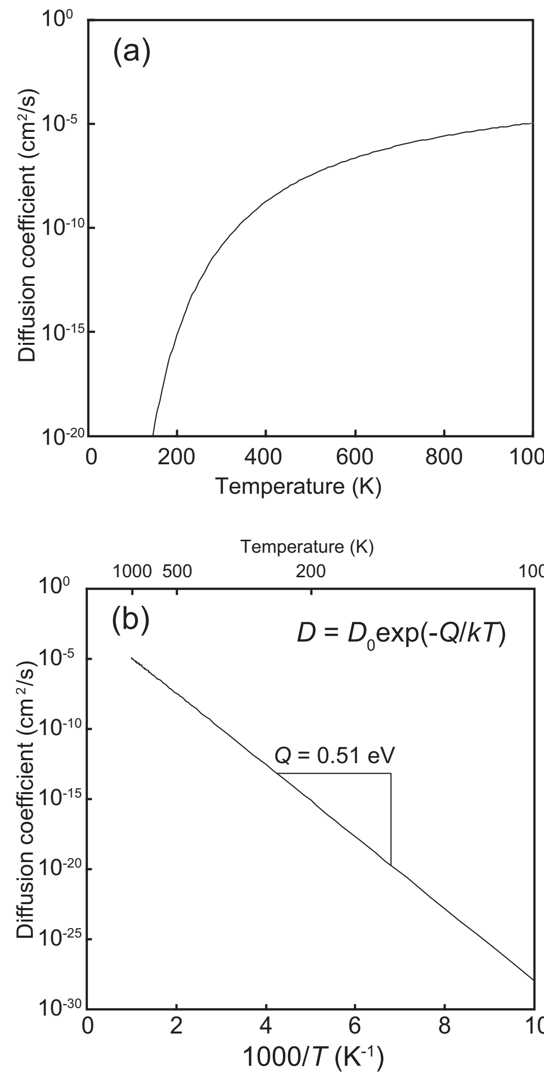

FIG. 6. Chemical diffusion coefficients of lithium atoms by the interstitial mechanism as a function of (a) temperature and (b) the inverse of temperature. The apparent activation energies Q in the range of 100–1000 K are shown in the figure.

B. Vacancy mechanism

1. Migration path and potential barrier

Figure 1(c) shows the schematic drawing of lithium migration by the vacancy mechanism. A vacancy is surrounded by six lithium atoms at second-nearest-neighbor hexagons and one of them jumps into the vacancy. Figure 7 shows the calculated migration path and the energy profile using the NEB method. A neighboring lithium atom does not migrate

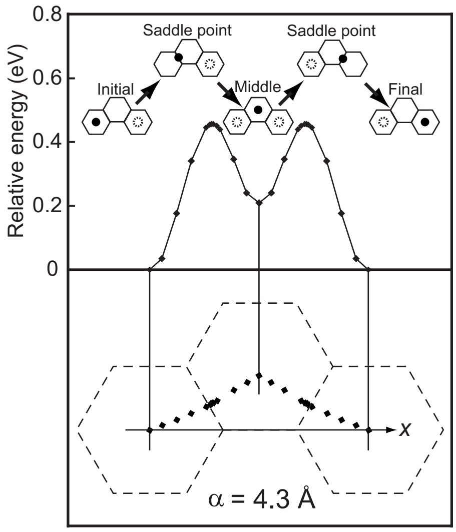

FIG. 7. (Bottom) Migration path and (top) energy profile along the path by the vacancy mechanism. The schematic drawings of the migration path are inserted in the figure. The hexagons denote the hexagonal network of carbon atoms [see also Fig. 1(c)].

in a straight-line trajectory but by way of a first-nearest-neighbor hexagon. The intermediated state corresponds to the metastable state energetically. There are two saddle-point states along the path, at which the migrating lithium atom is located on the borders of the two carbon hexagons. It is therefore necessary to estimate the two mean frequencies for the two elementary jumps; ω_{V1} corresponding to the jump from the initial regular site to the intermediated site (jump V1), and ω_{V2} corresponds to the following jump from the intermediated site to the final vacant site (jump V2). The calculated potential barriers ΔE^{mig} are 0.47 and 0.26 eV, respectively.

2. Change in vibrational free energy

Figure 8 shows the calculated phonon band structures and vibrational spectra at (a) the initial (equal to the final), (b) the saddle-point, and (c) the metastable (i.e., the final for jump V1 as well as the initial for jump V2) states. In the phonon spectra, the total spectrum (broken line) and the contribution of all the lithium atoms (solid line) and the migrating lithium atom (filled region) are shown. At the initial state, there are two major peaks of lithium atoms (peaks A and B), which are attributed to the in-plane and the perpendicular vibrations of lithium atoms, respectively. The contribution of one of the six lithium atoms neighboring to the vacancy has also two peaks (peaks a_V and b_V), whose positions and intensities are almost the same as those of peaks A and B. At the metastable state, the vibrational modes do not significantly change from those of the initial state except for broadening of the in-plane peak a_V. At the saddle-point state, one imaginary mode (peak a'_{V1}) appears, corresponding to the in-plane vibration in the migrating direction. The other in-plane mode is located at 2.6 THz (peak a'_{V2}), and this peak is lower than peak a_V at the initial state (7.2 THz). The perpendicular mode, in contrast, shows a broad peak at 24.4 THz (peak b'_V) on the higher-frequency side compared with that at the initial state.

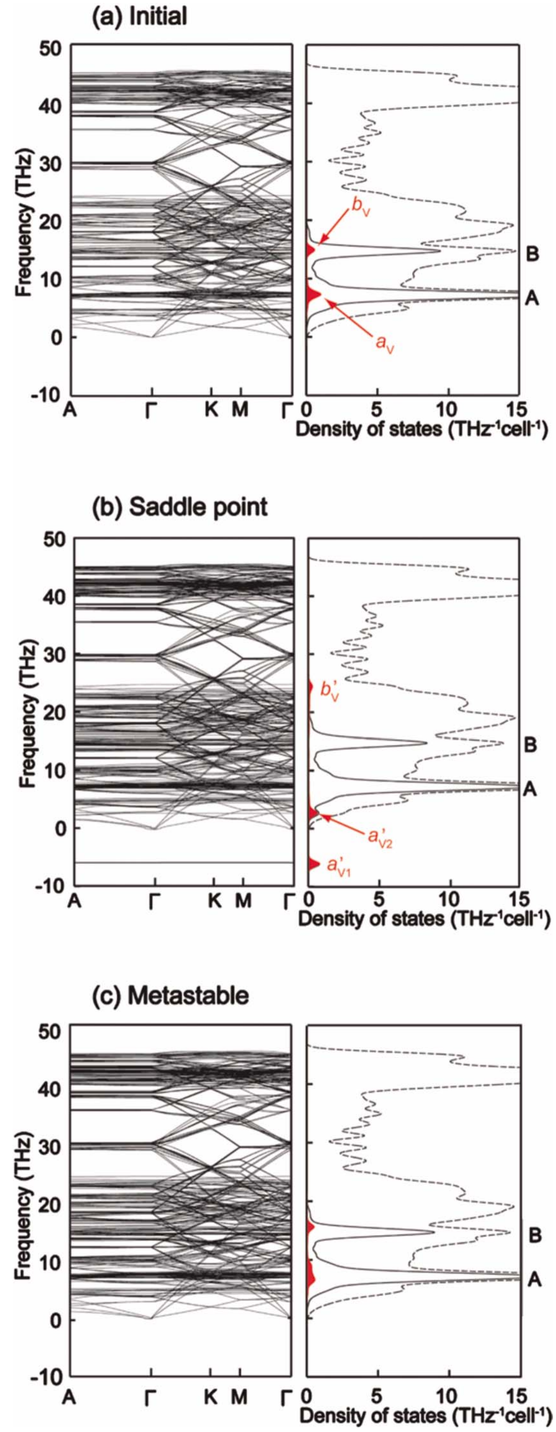

FIG. 8. (Color online) Calculated phonon band structures and vibrational spectra of (a) the initial, (b) the saddle-point, and (c) metastable states in the vacancy mechanism. The total spectrum, the contribution of all the lithium atoms, and that of the migrating lithium atom are expressed by broken line, solid line, and red filled region (indicated by arrows), respectively. Imaginary frequencies are expressed as negative values.

The changes in vibrational free energy ΔF^{vib} for jumps V1 and V2 are shown in Figs. 9(a) and 9(b), respectively. ΔF^{vib} of the two jumps are equivalent with a difference of less than 2 meV in this temperature range because the vibra-

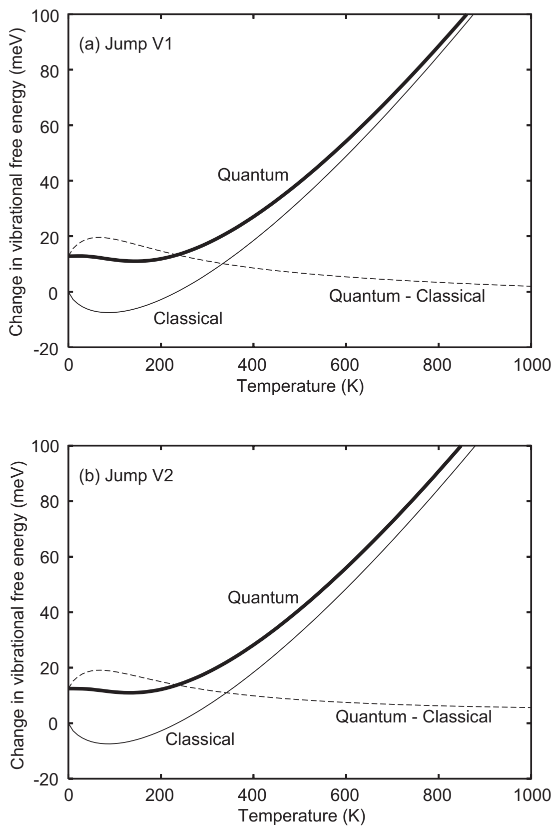

FIG. 9. Changes in vibrational free energy ΔF^{vib} for (a) jump V1 and (b) jump V2 as a function of temperature, evaluated in (thick lines) quantum and (thin lines) classical statistics. The discrepancies are also shown in the figures by broken lines.

tional spectra at the initial and metastable states have little difference. The discrepancies between quantum and classical statistics are also shown in the figures. They are 12–13 meV at 0 K, and remain 11–12 meV at room temperature.

3. Mean jump frequency and diffusion coefficient

Figure 10 shows the calculated mean jump frequencies for jumps V1 and V2 based on quantum statistics. ω_{V1} is much smaller than ω_{V2}, e.g., 4×10^{4} vs 1×10^{8} s^{-1} at room temperature. This is mainly caused by the difference in potential barrier between the two jumps (0.47 vs 0.26 eV). It is found that the first jump is rate determining in the vacancy mechanism.

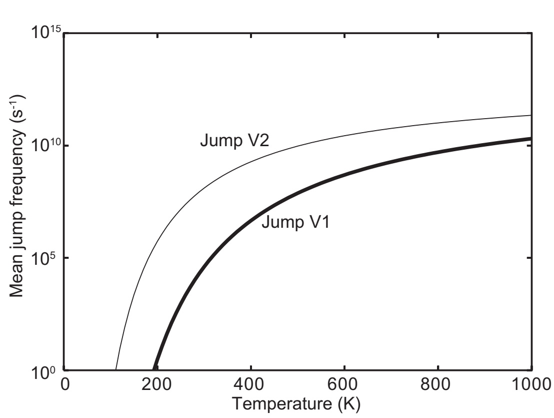

FIG. 10. Calculated mean frequencies of jumps V1 (ω_{V1}) and V2 (ω_{V2}) as a function of temperature using quantum statistics.

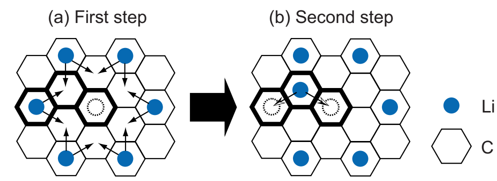

FIG. 11. (Color online) Possible elementary jumps for lithium atoms from the regular sites to a vacancy in LiC_6. The jump consists of two steps: (a) from the regular sites to the middle metastable sites, and (b) from the metastable sites to the vacant site.

It takes the total jump frequency of a vacancy, Γ_V, to estimate the chemical diffusion coefficient of lithium atoms in the lithium deficient case. The possible elementary jumps are schematically shown in Fig. 11. At the first step, there are 12 possible migration paths [Fig. 11(a)]. The migrating lithium atom at a metastable site can jump to either the vacant or the initial site [Fig. 11(b)]. The former jump means a successful jump, while the latter means failure. The mean time of the total jump is the sum of those of the individual steps, $\tau=\tau_1+\tau_2$, where $\tau_1=(12\omega_1)^{-1}$ and $\tau_2=(2\omega_2)^{-1}$. The factors of 12 and 2 are the numbers of possible jumps at the two steps as described above. Hence, the total jump frequency is given by $\Gamma_V=1/2\tau=(6\omega_1\omega_2)/(6\omega_1+\omega_2)$, where the factor of 1/2 is due to the success probability of the jump. If $\omega_1 \ll \omega_2$, the total jump frequency Γ_V can be approximated to $6\omega_1$. For example, the approximation ($6\omega_1$) is equivalent to the total frequency (Γ_V) within an error of 0.2% at room temperature while it overestimates Γ_V by more than 50% at 1000 K. Figure 12 shows D_{Li} by the vacancy mechanism as a function of (a) temperature and (b) the inverse of temperature. For instance, D_{Li} is 1×10^{-10} cm^2/s at room temperature, which is larger than that by the interstitial mechanism (1×10^{-11} cm^2/s). The apparent activation energy Q in the range of 100 and 1000 K is 0.49 eV, which is larger than the potential barrier of the first jump (0.47 eV) due to the change in zero-point vibrational energy.

IV. DISCUSSION

A. Vibrational mode

In this subsection, the vibrational modes at the initial and saddle-point states for each jump in the interstitial and vacancy mechanisms are discussed. First, the lattice vibration of the perfect crystal is explained for reference. The phonon spectrum of the perfect crystal is shown in Fig. 13(a). The broken and solid lines show the total spectrum and the contribution of lithium atoms, respectively. The contribution of lithium atoms has two peaks at 7 and 15 THz (peaks A and B) corresponding to the in-plane and perpendicular vibrations, respectively. These localized modes mean that all the lithium atoms in the perfect crystal are independent and not coupled with one another in terms of vibration. This is because each lithium atom is separately positioned in a lithium

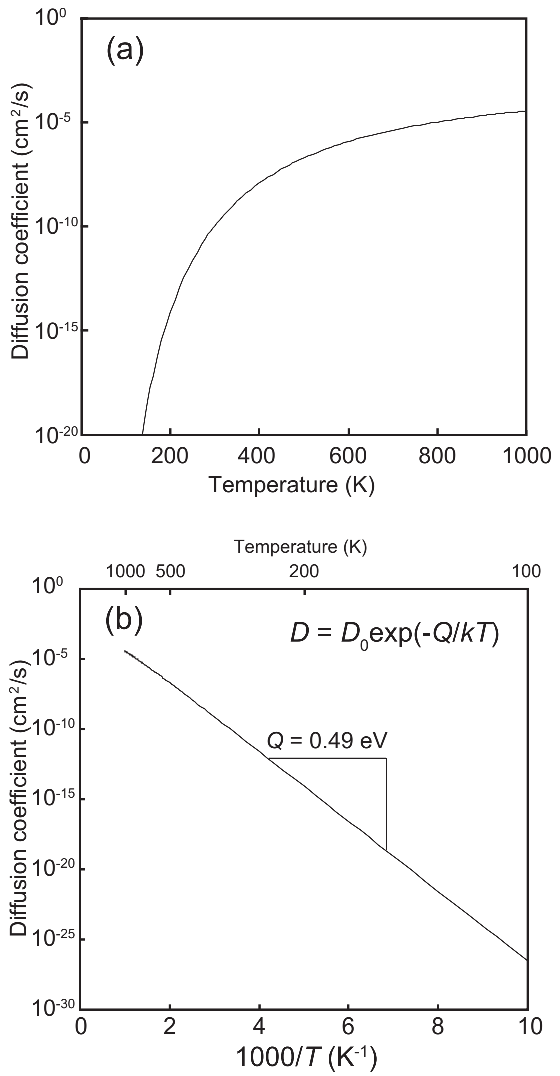

FIG. 12. Chemical diffusion coefficients of lithium atoms by the vacancy mechanism as a function of (a) temperature and (b) the inverse of temperature. The apparent activation energies Q in the range of 100–1000 K are shown in the figure.

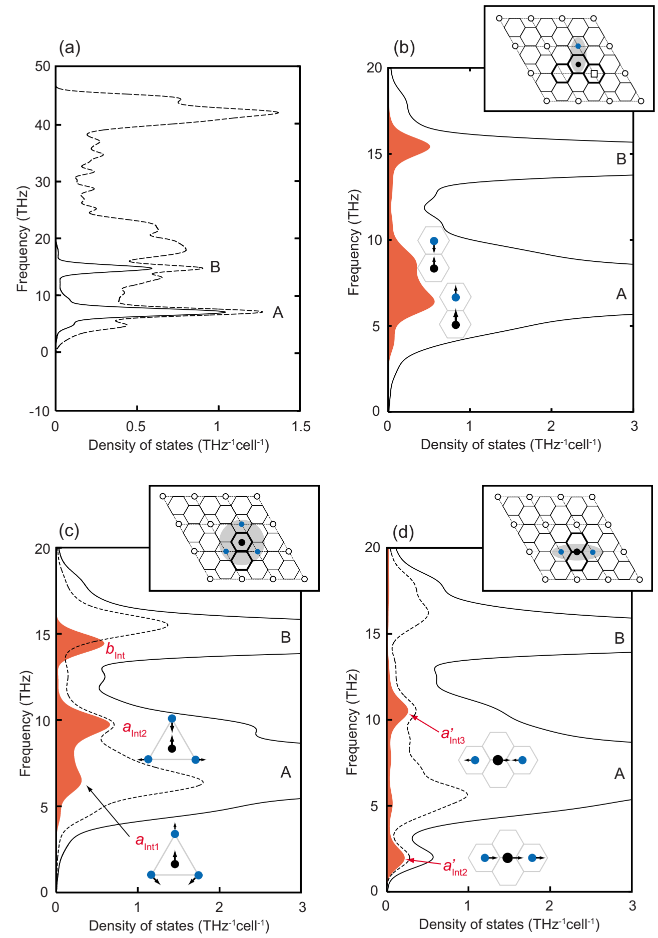

FIG. 13. (Color online) (a) The vibrational spectrum of the perfect crystal. The broken and solid lines show the total spectrum and the contribution of all the lithium atoms. The closeups of the vibrational spectra around peak A at (b) the metastable state in the vacancy mechanism, (c) the initial state, and (d) the saddle-point state in the interstitial mechanism. The solid line, filled region, and broken line show the contribution of all the lithium atoms, the migrating lithium atom, and the neighboring lithium atoms (three Li atoms at the initial or two Li atoms at the saddle point in the interstitial mechanism), respectively. The characteristic vibrational modes corresponding to each peak are also inserted in the figures.

layer. All the initial and saddle-point states for the jumps also have the two major peaks of lithium atoms at 7 and 15 THz (see Figs. 3 and 8). However, the vibrational modes of lithium atoms show some differences depending on the states for the jumps. Hereafter, the differences are discussed, particularly in the modes of the migrating lithium atom.

In the vacancy mechanism, all the lithium atoms at the initial state are not coupled with one another because they are separately positioned like in the perfect crystal. Therefore, the lithium contribution to the vibrational spectrum has little difference from that in the perfect crystal. At the metastable state, the migrating lithium atom occupies the intermediated site with one neighboring lithium atom at the first-nearest-neighbor hexagon. The peak corresponding to the in-plane vibration of the migrating lithium atom (peak a_V) broadens due to coupling with the neighboring lithium atom [Fig. 13(b)]. The lower-frequency side of the peak is attributed to the translational vibration of the interstitial and the neighboring lithium atom while the higher side is to the breathing vibration of the two lithium atoms (shown in the figure). At the saddle-point state, the migrating lithium atom is located on the borders of the two hexagons between the two C-C bonds. Hence, the vibrational modes of the migrating lithium atom drastically changes. First, one imaginary mode appears corresponding to the in-plane vibration along the migration path. Moreover, the other in-plane mode has lower frequency while the perpendicular mode has higher frequency, compared with those at the initial states. Considering that the migrating lithium atom at the saddle point is weakly coupled with the other lithium atoms, this tendency is the characteristic of a lithium atom on the borders of the hexagons.

In the interstitial mechanism, the migrating lithium atom, i.e., the interstitial, is strongly coupled with the lithium atoms at the neighboring hexagons. At the initial state, the lithium contribution to the vibrational spectrum has a shoulder on the high-frequency side at peak A, which does not appear in the cases of the perfect crystal and the vacancy mechanism. The closeup around peak A is shown in Fig. 13(c). The solid line, filled region, and broken line show the contributions of all the lithium atoms, the interstitial, and the three neighboring lithium atoms, respectively. The figure shows that the shoulder is mainly attributed to the lithium interstitial and also to the neighboring lithium atoms. The schematic drawings of the normal vibrational modes corresponding to peaks $a_{\mathrm{Int}\,1}$ and $a_{\mathrm{Int}\,2}$ are shown in the figure. In the vibration corresponding to peak $a_{\mathrm{Int}\,1}$, the three neighboring lithium atoms are displaced in the direction away from the interstitial. Peak $a_{\mathrm{Int}\,1}$ has the same frequency as the in-plane vibration of lithium atoms in the perfect crystal because the displacements of the neighboring lithium atoms reduce the electrostatic repulsion with the interstitial. On the contrary, peak $a_{\mathrm{Int}\,2}$ has higher frequency because the neighboring lithium atoms are displaced close to the interstitial with more repulsive interaction. At the saddle-point state, the in-plane mode of the migrating interstitial shows different trend from that in the case of vacancy mechanism because the interstitial is strongly coupled with the two neighboring lithium atoms [Fig. 13(d)]. The in-plane mode in the real frequency region is divided into the two peaks (peaks $a'_{\mathrm{Int}\,2}$ and $a'_{\mathrm{Int}\,3}$). The lower-frequency peak (peak $a'_{\mathrm{Int}\,2}$) corresponds to the translation of the three lithium atoms along the inline direction. It has almost the same frequency as that at the saddle-point state in the vacancy mechanism. This is because the two neighboring lithium atoms are displaced to reduce their repulsive interaction. The higher peak (peak $a'_{\mathrm{Int}\,3}$) is due to the asymmetric stretching with strong repulsion between the interstitial and the neighboring lithium atoms.

B. Change in vibrational free energy

The change in vibrational free energy ΔF^{vib} can be evaluated using Eq. (15) based on quantum statistics or the classical approximation of Eq. (16). ΔF^{vib} for jumps Int, V1, and V2 are shown in Fig. 4 and Figs. 9(a) and 9(b), respectively. The changes in vibrational free energy for the three jumps show the same tendency. Therefore the interstitial jump (jump Int) is focused hereafter.

At 0 K, the quantum ΔF^{vib} is a positive finite value (13 meV) corresponding to the change in zero-point vibrational energy $\Delta E^{\mathrm{vib}}_{\mathrm{zero}}$ from the initial to the saddle point. Note that the vibrational free energy at the initial is evaluated with $3N$ degrees of freedom while that at the saddle point is with $3N-1$ degrees. The positive $\Delta E^{\mathrm{vib}}_{\mathrm{zero}}$ means that the increase in the frequencies of the $3N-1$ vibrational modes at the saddle-point state outweighs the decrease in number of the modes. The classical ΔF^{vib} is exactly zero, and the difference from the quantum one is equal to the change in zero-point vibrational energy. With increasing temperature, the quantum ΔF^{vib} decreases in the low-temperature range. In this range, high-frequency vibrational modes are not thermally excited, and only low-frequency modes make a major contribution to the temperature dependence of vibrational free energy. This downward tendency means that the saddle-point state has many low-frequency modes compared with the initial. Actually, the in-plane vibration of the migrating lithium atom at the saddle point has lower frequency (peak $a'_{\mathrm{Int}\,2}$) than that at the initial (peaks $a_{\mathrm{Int}\,1}$ and $a_{\mathrm{Int}\,2}$). With further increase in temperature, ΔF^{vib} show the upward tendency in the high-temperature range. This is derived from the difference in number of the vibration modes of the migrating lithium atom; three at the initial versus two at the saddle point. This difference influences ΔF^{vib} only at enough high temperatures to excite the in-plane vibration of the migrating lithium atom at the initial state (7 THz; around 300 K in temperature equivalent). The discrepancy between quantum and classical statistics is large in the low-temperature range mainly due to the zero-point vibrational energy and the low-frequency modes, while the classical value gradually converges to the quantum one at temperatures higher than room temperature.

C. Mean jump frequency

In this subsection, the difference in mean jump frequency between quantum and classical statistics is discussed. Mean jump frequencies under quantum statistics essentially deviate from the Arrhenius form, unlike in the case of the classical approximation [Eq. (2)]. How should the jump frequencies ω be related to the parameters in the Arrhenius equation, the vibrational prefactor ν^*, and the apparent activation energy q?

The activation energy q can be defined from the gradient of the Arrhenius plot as

$$q = -\frac{\partial(\ln \omega)}{\partial(1/kT)} = \Delta E^{\mathrm{mig}} + \Delta E^{\mathrm{vib}} + kT. \tag{17}$$

ΔE^{vib} can be separated into $\Delta E^{\mathrm{vib}}_{\mathrm{zero}}$ and the rest term depending on temperature, $\Delta E^{\mathrm{vib}}_{T}(T)$,

$$\Delta E^{\mathrm{vib}} = \Delta E^{\mathrm{vib}}_{\mathrm{zero}} + \Delta E^{\mathrm{vib}}_{T}, \tag{18}$$

$$\Delta E^{\mathrm{vib}}_{T} = \sum_{i=1}^{3N-1} \frac{h\nu_i^S}{\exp(h\nu_i^S/kT) - 1} - \sum_{i=1}^{3N} \frac{h\nu_i^I}{\exp(h\nu_i^I/kT) - 1}. \tag{19}$$

The vibrational prefactor ν^* can be expressed as

$$\nu^* = \omega/\exp\left(-\frac{q}{kT}\right) = \frac{kT}{h}\exp\left(1 + \frac{\Delta S^{\mathrm{vib}}}{k}\right), \tag{20}$$

Figures 14(a) and 14(b) show the changes in vibrational energy, ΔE^{vib}, and in vibrational entropy, ΔS^{vib}, for the interstitial jump (jump Int). ΔE^{vib} is a finite value at 0 K corresponding to the zero-point vibrational energy. With increasing temperature, it slightly increases up to 100 K and decreases at higher temperatures. ΔS^{vib} has almost the same tendency as ΔE^{vib} except for the difference in value at 0 K. This temperature dependence is derived from the difference in number of the excited modes between the initial and saddle-point states, as already discussed in Sec. IV B. At high temperature, the energy and entropy of a harmonic

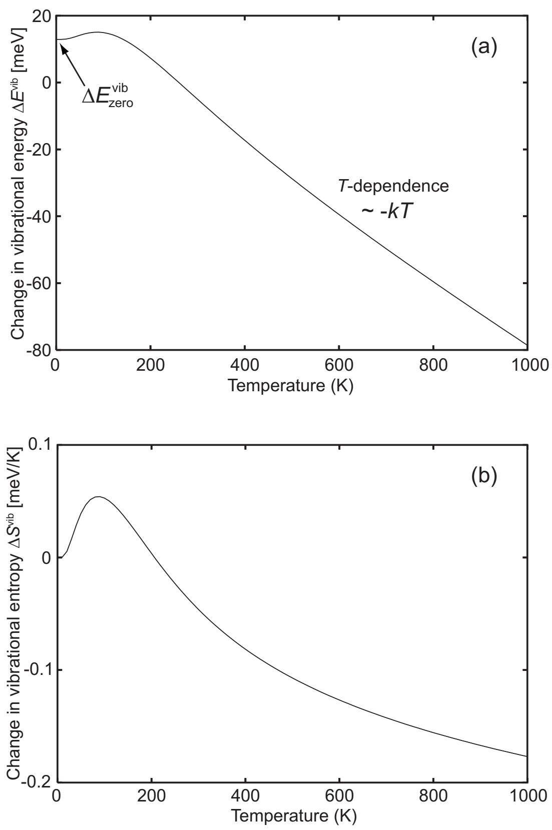

FIG. 14. Changes in (a) vibrational energy $\Delta E^{\rm vib}$ and (b) vibrational entropy for the interstitial jump (jump Int).

oscillator can be expressed by the following classical approximation:

$$E^{\rm vib}(\nu) \to kT \quad (T \to \infty), \tag{21}$$

$$S^{\rm vib}(\nu) \to k \ln\left(\frac{kT}{h\nu}\right) + k \quad (T \to \infty). \tag{22}$$

Taking the difference in number of the vibrational modes between the initial and saddle-point states into account, $\Delta E^{\rm vib}$ converges to $-kT$ at high temperatures and cancels the term of $+kT$ in Eq. (17). Therefore, q is equal to $\Delta E^{\rm mig}$ at the high-temperature limit. This means that the expression of Vineyard[10] is equal to the high-temperature limit. The convergence of $\Delta S^{\rm vib}$ depends on the frequencies of the normal vibrational modes at the initial and saddle-point states as follows:

$$\Delta S^{\rm vib}(\nu) \to k \ln\left(\frac{h}{kT}\frac{\prod_{i=1}^{3N}\nu_i^I}{\prod_{i=1}^{3N-1}\nu_i^S}\right) - k \quad (T \to \infty). \tag{23}$$

By comparison between Eqs. (20) and (23), the vibrational prefactor ν^* converges to the classical expression by Vineyard[10] at high temperatures.

Figure 15 shows the activation energies q and the vibrational prefactors ν^* for each jump defined as the above equations. The broken lines show the classical limits (high-temperature limits). With respect to the activation energies q, each of them at 0 K corresponds to the sum of the potential barrier and the change in zero-point vibrational energy. With increasing temperature, q increases with the gradient of k in the vicinity of 0 K, derived from the kT term in Eq. (17). The lattice vibrations are not excited and $\Delta E^{\rm vib}$ has little temperature dependence at the low temperatures. The upward trend of the kT term is canceled out around 150 K by the downward trend of $\Delta E^{\rm vib}$ approximated to be $-kT$ at high temperatures. With further increase in temperature, q gradually converges to the classical limit of $\Delta E^{\rm mig}$ (not $\Delta E^{\rm mig}+\Delta E^{\rm vib}_{\rm zero}$). In this temperature range (0–1000 K), the activation energies q do not converge to the classical limits and the discrepancies remain comparable to the changes in zero-point vibrational energy $\Delta E^{\rm vib}_{\rm zero}$. With regard to the vibrational prefactors ν^*, the same tendency can be seen as the activation energies q. At 0 K, each of them starts at 0 $\rm s^{-1}$ due to the term of kT/h in Eq. (20), and rapidly increases with the gradient of k/h in the vicinity of 0 K. Over 150 K, kT/h is canceled out by the inverse temperature dependence of $\Delta S^{\rm vib}$. With increasing temperature, ν^* gradually converge to the classical-limit values. The classical approximation underestimates ν^* by 30% at room temperature and by 5% at 1000 K.

V. CONCLUSIONS

In summary, we have investigated the lithium diffusion by the interstitial and vacancy mechanisms in LiC_6 from first principles. Based on transition state theory, the mean frequencies of the possible jumps in LiC_6 have been rigorously evaluated from the corresponding potential barriers and lattice vibrations. The potential barriers in the interstitial and vacancy mechanisms are almost the same: 0.48 eV for the interstitial jump vs 0.47 eV for the rate determining jump in the vacancy mechanism. The mean jump frequencies per path are almost the same between the two mechanisms. The calculated chemical diffusion coefficients of lithium atoms at room temperature are 1×10^{-11} $\rm cm^2/s$ by the interstitial mechanism and 1×10^{-10} $\rm cm^2/s$ by the vacancy mechanism. There are many reports on the measurements of the lithium chemical diffusion at room temperature using electrochemical techniques, such as alternating-current (ac) impedance measurements and potentiostatic and galvanostatic intermittent titration techniques (PITT and GITT).[15] Our calculated values are in the wide range of these reported values from 10^{-7} to 10^{-12} $\rm cm^2/s$.

With regard to the vibrational modes, all the lithium atoms in the perfect crystal are independent and not coupled with one another in terms of vibration due to their separated positions. The lithium atoms are weakly coupled with one another during the migration in the vacancy mechanism while the migrating lithium atom in the interstitial mechanism is strongly coupled with the neighboring lithium atoms. The apparent activation energies for the mean jump frequencies under quantum statistics are larger than the potential barriers (corresponding to the classical approximation) by the changes in zero-point vibrational energy at low temperatures. The discrepancies between quantum and classical sta-

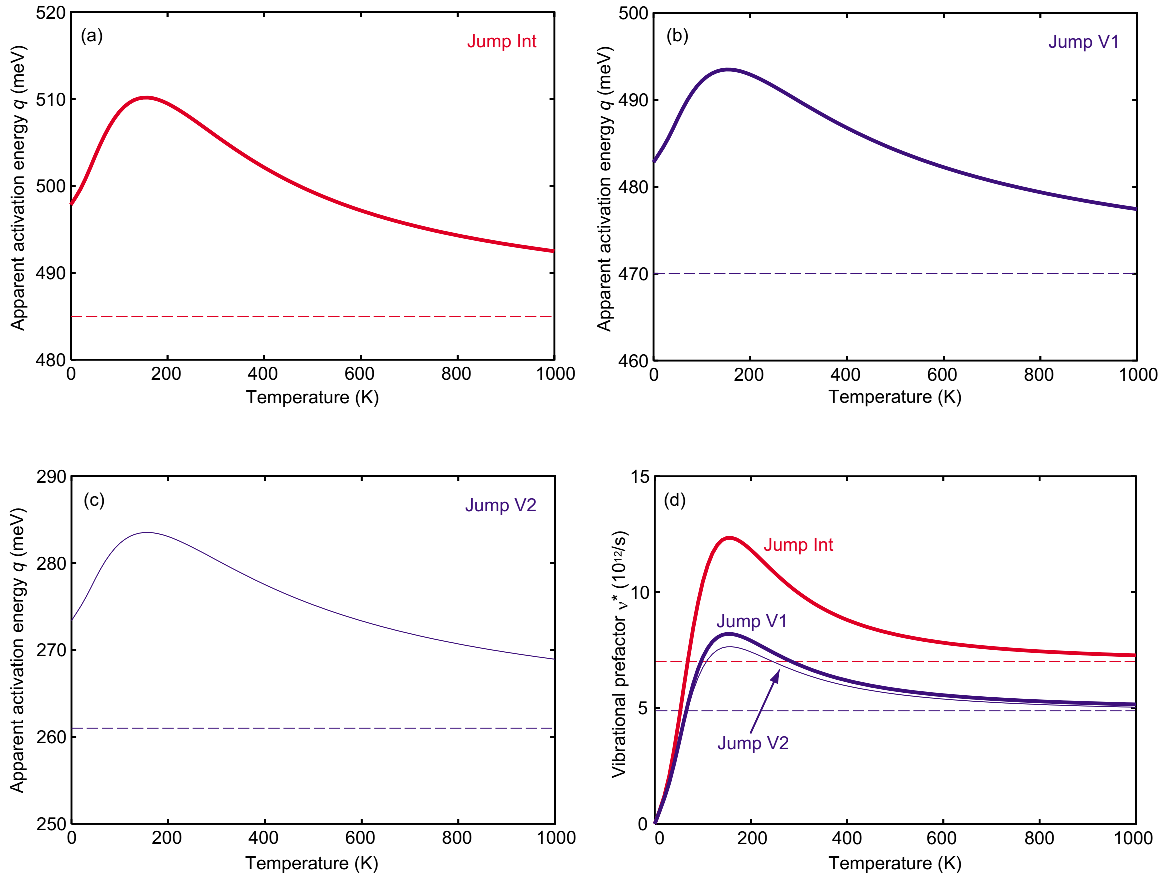

FIG. 15. (Color online) Apparent activation energies q for (a) jump Int, (b) jump V1, and (c) jump V2. The broken lines show the potential barriers ΔE^{mig} corresponding to the classical limits. (d) Vibrational prefactors ν^* for Jumps Int, V1, and V2 as a function of temperature.

tistics remain comparable to the changes in zero-point vibrational energy even at 1000 K. The vibrational prefactors under quantum statistics also deviate from the values using the classical approximation. The factors under quantum statistics are much smaller than the classical values at low temperatures while they rapidly converge to the classical limits with increasing temperatures. The classical approximation underestimates ν^* by 30% at room temperature and by 5% at 1000 K.

ACKNOWLEDGMENTS

The authors would like to thank H. Numakura and A. Togo for helpful discussions. This work was supported by three programs from the Ministry of Education, Culture, Sports, Science, and Technology of Japan: the Grant-in-Aids for Scientific Research (A) and Priority Area on "atomic scale modification" (Contract No. 474), and the global COE program. K.T. also thanks the Japan Society for the Promotion of Science.

*k.toyoura@t01a0005531.mbox.media.kyoto-u.ac.jp
†tanaka@cms.mtl.kyoto-u.ac.jp

[1] P. G. Shewmon, *Diffusion in Solids* (McGraw-Hill, New York, 1963); Th. Heumann, *Diffusion in Metallen* (Springer-Verlag, Berlin, 1992).
[2] R. Car and M. Parrinello, Phys. Rev. Lett. **55**, 2471 (1985).
[3] P. E. Blöchl, E. Smargiassi, R. Car, D. B. Laks, W. Andreoni, and S. T. Pantelides, Phys. Rev. Lett. **70**, 2435 (1993).
[4] S. Glasstone, K. J. Laidler, and H. Eyring, *The Theory of Rate Processes* (McGraw-Hill, New York, 1941); P. Hänggi, P. Talkner, and M. Borkovec, Rev. Mod. Phys. **62**, 251 (1990).
[5] D. J. Wales, Int. Rev. Phys. Chem. **25**, 237 (2006).
[6] G. Henkelman, B. P. Uberuaga, and H. Jónsson, J. Chem. Phys. **113**, 9901 (2000).
[7] W. Frank, U. Breier, C. Elsässer, and M. Fähnle, Phys. Rev. Lett. **77**, 518 (1996).
[8] A. Van der Ven, G. Ceder, M. Asta, and P. D. Tepesch, Phys. Rev. B **64**, 184307 (2001).
[9] F. Montalenti, D. B. Migas, F. Gamba, and L. Miglio, Phys. Rev. B **70**, 245315 (2004).

[10] G. H. Vineyard, J. Phys. Chem. Solids **3**, 121 (1957).
[11] A. Van der Ven and G. Ceder, Phys. Rev. Lett. **94**, 045901 (2005).
[12] C.-O. Hwang, J. Chem. Phys. **125**, 226101 (2006).
[13] T. Vegge, Phys. Rev. B **70**, 035412 (2004).
[14] L. T. Kong and L. J. Lewis, Phys. Rev. B **74**, 073412 (2006).
[15] Z. Ogumi and M. Inaba, Bull. Chem. Soc. Jpn. **71**, 521 (1998); M. D. Levi, E. Markevich, and D. Aurbach, Electrochim. Acta **51**, 98 (2005); Y. NuLi, J. Yang, and Z. Jiang, J. Phys. Chem. Solids **67**, 882 (2006).
[16] S. A. Safran, Solid State Phys. **40**, 183 (1987).
[17] D. S. Robinson and M. B. Salamon, Phys. Rev. Lett. **48**, 156 (1982).
[18] K. C. Woo, H. Mertwoy, J. E. Fischer, W. A. Kamitakahara, and D. S. Robinson, Phys. Rev. B **27**, 7831 (1983); J. E. Fischer, C. D. Fuerst, and K. C. Woo, Synth. Met. **7**, 1 (1983).
[19] R. Gomer, Rep. Prog. Phys. **53**, 917 (1990); G. E. Murch, in *Phase Transformations in Materials*, edited by G. Kostorz (Vch Verlagsgesellschaft Mbh, Germany, 2001), p. 171.
[20] P. E. Blöchl, Phys. Rev. B **50**, 17953 (1994); G. Kresse and J. Hafner, *ibid.* **47**, 558 (1993); **48**, 13115 (1993); **49**, 14251 (1994).
[21] J. P. Perdew and A. Zunger, Phys. Rev. B **23**, 5048 (1981).
[22] H. J. Monkhorst and J. D. Pack, Phys. Rev. B **13**, 5188 (1976).
[23] A. Togo, http://fropho.sourceforge.net/, FROPHO: Frozen Phonon analyzer for periodic boundary-condition materials, 2006.